9-2001

# On Misorientation Distribution Evolution During Anisotropic Grain Growth

Elizabeth A. Holm
*Sandia National Laboratories*

Gregory N. Hassold
*Kettering University*

Mark A. Miodownik
*King's College London*

Pergamon

Acta mater. (2001) ••–••

Acta MATERIALIA

www.elsevier.com/locate/actamat



# ON MISORIENTATION DISTRIBUTION EVOLUTION DURING ANISOTROPIC GRAIN GROWTH

**E. A. HOLM[1]†, G. N. HASSOLD[2] and M. A. MIODOWNIK[3]**

[1]Materials and Process Modeling, Sandia National Laboratories, PO Box 5800, Albuquerque, NM 87185-1411, USA, [2]Department of Science and Mathematics, Kettering University, Flint, MI 48504, USA and [3]Department of Mechanical Engineering, King's College London, London, UK

*( Received 27 October 2000; received in revised form 13 May 2001 )*

**Abstract**—In order to study the development of texture and boundary character during annealing, three-dimensional grain crystallography and crystallographically mediated grain boundary properties were incoporated into a finite temperature Monte Carlo model for grain growth. Randomly textured microstructures evolve normally, with growth exponent $n = 0.96$. While texture remains random, the steady-state boundary misorientation distribntion favors low-angle boundaries. To first order, low-angle boundaries increase by lengthening, not by proliferating. In contrast, microstructures with a strong single-component texture develop four-grain junctions and highly curved grain boundaries, which alter evolution. The boundary misorientation distribution narrows and shifts to low angles, and no steady state is observed. The accompanying decrease in mean boundary mobility causes growth to slow, resulting in a growth exponent $n = 0.62$. The dependence of the growth exponent on average boundary mobility may explain experimental observations of exponents less than unity. *© 2001 Published by Elsevier Science Ltd on behalf of Acta Materialia Inc.*

*Keywords:* Grain growth; Computer simulation; Grain boundaries; Microstructure; Texture

## 1. INTRODUCTION

It is well known that crystallographic texture plays an important role in determining the physical, electrical and magnetic properties of polycrystalline materials. Some properties (e.g., plasticity) are affected by the bulk texture; others (e.g., high-temperature superconductivity) are influenced by the distribution of grain boundary types, which is texture-mediated. Controlling both texture and grain boundary character is therefore very important during processing of metal alloys.

Grain boundary engineering [1] is an ambitious application of thermomechanical processing to optimize both texture and boundary character. Tantalizing evidence of the effectiveness of this approach has been provided by Palumbo *et al.* [2, 3], who have developed processing routes that dramatically improve the corrosion resistance of certain alloys by increasing the fraction of coincident site lattice (CSL) boundaries present in the microstructure. During grain boundary engineering, an increase in CSL boundaries is often accompanied by a decrease in intensity of the bulk texture, illustrating the complex relationship between texture and boundary character.

Traditional X-ray analysis has long been used to measure the global frequency distribution of grain orientations in a polycrystal [i.e., the orientation distribution function (ODF) or texture], and grain misorientation distribution functions (MDFs) have been derived in various ways from the ODF. Recent advances in orientation imaging microscopy (OIM) [4] produce detailed, spatial maps of crystallographic orientations. This allows, for the first time, easy calculation of the frequency distribution of actual grain boundary misorientations in real polycrystals. This grain boundary MDF is not derived from the ODF, but rather is directly measured for each boundary in a microstructure and so depends explicitly on neighbor grain correlations. In fact, there is no unique relationship between an ODF and its grain boundary MDF; a given ODF can result in very different MDFs, depending on grain correlations [5]. In this paper, all referenced MDFs are of the directly measured, grain boundary type.

Automated OIM techniques enable detailed investigations of the influence of microstructural evolution on both the ODF and the MDF. However, because there is yet little understanding of the fundamental mechanisms that control the evolution of boundary character, annealing schedules to optimize the MDF continue to be developed empirically.

† To whom all correspondence should be addressed. Fax: +1-505-844-9781.

*E-mail address:* eaholm@sandia.gov (E. A. Holm)

1359-6454/01/$20.00 © 2001 Published by Elsevier Science Ltd on behalf of Acta Materialia Inc.
PII: S1359-6454(01)00207-5

Polycrystalline microstructures include a menagerie of microstructural features: grain boundaries, second-phase particles, dislocations, solute, etc. Since microstructural evolution depends upon the local topology and connectivity of these features, mesoscale computer simulations for microstructural evolution can provide valuable insight. The most successful mesoscale grain growth models include Potts models [6], front tracking models [7], vertex models [8], phase field models [9], and cellular automata [10]. The kinetics and topological characteristics of isotropic grain growth have been exhaustively investigated using these methods.

Relatively little work has been done to investigate the effects of anisotropic boundary properties on the evolution of texture and the MDF. Grest *et al.* [11] used the Potts model to simulate the effect of misorientation-dependent boundary energy on grain growth. In that study, crystal orientations were not three-dimensional, but rather were scalar tilt angles, which unconstrains the formation of low-energy boundaries. In addition, the results suffered from simulation lattice pinning, which affected both microstructure and evolution kinetics. Subsequent Potts model studies of anisotropic grain growth have also attempted to incorporate crystallography [12–17], usually to probe the coupling between texture development and abnormal grain growth [12–15, 17]. Most of these simulations utilize scalar crystallography [12, 13, 15, 17]. Some restrict the effects of crystallography to boundary mobility (not energy) [15, 17], or do not weight boundary mobility by energy [12–14, 16]. Others operate on non-statistical system sizes and simulation times [16] or may be affected by lattice pinning [14]. In addition, most of these studies specify an initial condition tailored to initiating the phenomenon of interest (e.g., seeding the microstructure with special grains) [12, 13, 15, 17]. Thus the aim of this paper is twofold: (1) to discuss the incorporation of misorientation-dependent boundary properties in Potts model simulations, and (2) to investigate the development of texture and MDF during grain growth.

The paper is set out in the following way. First we examine the crystallography of polycrystalline microstructures and review the experimental measurements of energetic and kinetic parameters required to characterize the microstructure. Then we discuss how these parameters can be implemented into the Potts model simulation. Finally we describe two examples of anisotropic grain growth, the evolution of a random texture and the evolution of a strong single-component texture. When discussing these examples we focus on the changes in the MDF caused by grain growth.

## 2. CRYSTALLOGRAPHY AND BOUNDARY PROPERTIES

### 2.1. *Orientation and misorientation*

The orientation of the axes of a crystal with respect to an external frame of reference (the specimen axes) can be specified by a rotation in three-dimensional space (posessing three degrees of freedom). As such it can be represented by a (3×3) rotation matrix **O**. The misorientation between two grains is the rotation that rotates one grain's orientation into that of the other. If the orientation of grain $A$ is represented by the rotation matrix $\mathbf{O}_A$, and that of grain $B$ by $\mathbf{O}_B$, then the misorientation rotation matrix **M** is given by $\mathbf{M} = \mathbf{O}_A\mathbf{O}_B^{-1}$. There are several equivalent ways of representing this misorientation rotation. A popular choice is the angle/axis description, in which an axis $\boldsymbol{l}$ (a unit vector) and a scalar rotation angle $\theta$ are specified. In this study we only consider cubic crystallography which, due to symmetry of the orientation space, has 24 geometrically equivalent representations of any rotation. Therefore there are 24 equivalent angle/axis pairs that describe the misorientation rotation. By convention we select the angle/axis pair with the smallest rotation angle. Since the axis is usually ignored when discussing boundary properties, the misorientation is then characterized by the minimum rotation angle $\theta$. This approach ignores the other degrees of freedom of the boundary: two associated with the orientation of the axis $\boldsymbol{l}$, and two more with the orientation of the boundary plane (which can be specified by its unit normal). It is expected that the boundary structure and properties will be dependent on these parameters; however, since there is no general model to describe the functional dependence, we follow convention and characterize boundary properties as a function of $\theta$ alone.

The CSL description of grain boundaries is a geometric model based on the fact that, for certain misorientation rotations, a fraction of the atomic lattice sites will be coincident at the boundary [18, 19]. The CSL misorientation relationship is characterized by a rotation matrix or angle/axis pair. CSL boundaries are seldom observed in general materials, as CSL formation requires three independent orientation relationships to be satisfied. Brandon [20] introduced the concept of an acceptance criterion, which allows a wider range of misorientations to be classified as a particular CSL boundary. The importance of CSL boundaries on grain growth is unclear; while they undoubtedly possess special boundary properties, their rarity diminishes their impact. Ono *et al.* [16], however, report an increase in the number of CSLs in anisotropic grain growth simulations. We address this issue fully in a subsequent paper; for the moment we are content to exclude CSLs from our model.

### 2.2. *Boundary energy*

Read and Shockley [21] derived an analytical expression for the free energy (per unit area) of a low-angle grain boundary. The boundary is assumed to be comprised of a regular array of dislocations. The boundary energy can be expressed as a function of the misorientation angle $\theta$:

$$\gamma = \gamma_0\theta(A - \ln\theta), \qquad (1)$$

where $\gamma_0$ and $A$ are related to elastic constants and properties of the dislocation cores. Here, $\gamma_0$ sets the overall energy scale, and $A$ adjusts the angle of the maximum grain boundary energy. For high-angle grain boundaries, this model would not be expected to be valid, as the dislocation cores would overlap substantially, and core interactions could not be neglected. To model boundary energy over the entire range of $\theta$, it is often assumed that high-angle boundaries are similar to one another, and they are given a uniform, high boundary energy. Thus a normalized model for the energy of a general grain boundary incorporates both equation (1) and a high-angle assumption:

$$\gamma = \begin{cases} \dfrac{\theta}{\theta_m}\left[1 - \ln\left(\dfrac{\theta}{\theta_m}\right)\right], & \theta < \theta_m \\ 1, & \theta \geq \theta_m \end{cases} \tag{2}$$

where $\theta_m$ is the misorientation angle that results in the maximum (in this case, unit) boundary energy. Experimentally $\theta_m$ is observed to lie between 10° and 30°, depending on the material [19].

### 2.3. Boundary mobility

According to linearized rate theory, the velocity of a boundary moving by curvature-driven growth is proportional to its curvature such that

$$v = M\kappa, \tag{3}$$

where $\kappa$ is the mean curvature and $M$ is the reduced mobility. $M$ is itself a product of two terms, the boundary mobility $\mu$ and the grain boundary energy $\gamma$. The reduced mobility is used in equation (3) for the practical reason that it is difficult to obtain independent experimental measurements of $\mu$ and $\gamma$. Gottstein *et al.* have studied curved boundaries in bicrystals to measure the misorientation dependence of the reduced mobility [22]. The same group has pioneered a technique for measuring absolute boundary mobility under a magnetic driving force in magnetically anisotropic bicrystals [23]. While significant progress has been made (such as the discovery of the compensation effect), a general relationship between misorientation and reduced mobility has neither been discovered nor predicted theoretically.

Because $\mu$ is poorly characterized compared with $\gamma$, in this study we generally ignore the effect of $\mu$ (i.e., set $\mu = 1$), so that $M = \gamma$. While this approach is not quantitatively accurate, it captures the qualitative results observed in most experiments. Mobility is very small for low-misorientation boundaries and increases with misorientation up to some fairly uniform high-angle value. While studies of subgrain boundary mobility show a more severe dependence of $M$ on $\theta$ than equation (2) predicts [24], the trends are generally correct. Moreover, our parametric studies of various functional forms for $M$ indicate that qualitatively similar mobility functions give quantitatively similar results; mobility functions that increase steeply at low angles and level off at high angles [as equation (2)] produce virtually identical structures and dynamics during microstructural evolution.

## 3. SIMULATION METHODOLOGY

### 3.1. The algorithm

A continuum microstructure is bitmapped on to a discrete lattice. Each lattice site is allocated an index $s_i$ so that all sites within a grain have the same index, and grain boundaries are represented by interfaces between neighboring sites of unlike index. Each index is also assigned a discrete crystallographic orientation $\mathbf{O}_i$ using a method that allows both the initial texture and MDF of the ensemble to be defined from experimental measurements [5]. The misorientation angle between grains $i$ and $j$, $\theta_{ij}$, is the minimum misorientation angle between orientations $\mathbf{O}_i$ and $\mathbf{O}_j$, as discussed in Section 2.1. The grain boundaries have a misorientation-dependent excess energy $\gamma(\theta_{ij})$ given by equation (2). This allows us to specify the total system energy by the Hamiltonian:

$$H = \sum_{i=1}^{N} \sum_{j=1}^{n} \gamma(\theta_{ij}), \tag{4}$$

where the sums are taken over the $n$ sites within the neighbor shell of site $i$ and for all $N$ lattice sites.

Because nucleation of new grain orientations is not a process we wish to study here, we select a grain growth algorithm that utilizes only grain boundary motion to evolve the microstructure; no nucleation events are allowed. Grain growth is simulated by selecting a site at random and choosing a candidate index from the set of neighbor indices. (Note that the index selection is not weighted by the number of neighbors possessing that index.) The change in system energy for flipping the site to the candidate index is calculated by using equation (4). The flip is performed with probability $P(\Delta E)$ given by

$$P(\Delta E) = \begin{cases} p_0, & \Delta E \leq 0 \\ p_0 \exp(-\Delta E/kT), & \Delta E > 0 \end{cases} \tag{5}$$

where

$$p_0 = \frac{M(\theta_{ij})}{M_m}. \tag{6}$$

$M(\theta_{ij}) = \gamma(\theta_{ij})$ is the reduced mobility of the boundary between grains $i$ and $j$. $M_m$ is the maximum mobility in the system, thus an index flip is accepted with a probability proportional to the normalized boundary mobility [25]. k$T$ is an energy defining the thermal fluctuation of the simulation and in practice determines the amount of noise present in the system. After each flip attempt, the time clock is incremented by $1/(NQ)$ Monte Carlo steps per site per index (MCSS), where $Q$ is the number of allowed orientations. (Scaling the conventional Monte Carlo time clock by $Q$ allows simulations with different $Q$ values to be directly compared.) This same Potts model algorithm has been shown to produce boundary motion by curvature, so that each boundary in the system moves according to the motion law given in equation (3) [26].

### 3.2. *Lattice pinning*

Consider a boundary connecting two points separated by distance $d$. On a square lattice the boundary will incorporate fewer segments if it lies in a ⟨01⟩ direction ($d$ segments) than if it lies in a ⟨11⟩ direction ($\sqrt{2}d$ segments). Since kinetic Monte Carlo models minimize system energy by decreasing boundary length, there is a driving force to place boundaries along lattice facets. This results in grain shapes that mimic the underlying lattice symmetry and growth kinetics that slow or stop as evolution progresses [27, 28]. These lattice effects are more pronounced in systems that require fine distinctions in boundary energy [29], in three-dimensional systems and in systems with other pinning mechanisms [28]. Since these lattice effects are non-physical, it is necessary to eliminate them from grain growth simulations.

Lattice effects operate by faceting boundaries. They can be overcome by injecting a sufficient number of steps on to the boundaries. Then, step flow processes can allow the boundary to find and track its energetically favored position, restoring correct grain junction angles and permitting free boundary motion.

In practice, lattice effects are mitigated in two ways [27]. Increasing the neighbor sampling per site [i.e., by adding additional shells of interacting neighbors in equation (4)] decreases the energetic anisotropy of the lattice. Increasing the simulation temperature $T$ activates thermal fluctuations that roughen the boundaries. Given a lattice, the correct $T$ is found by trial and error. Generally, $T$ is increased until grains are equiaxed, junction angles are correct, and growth kinetics converge. It should be noted that $T$ must not be construed as being a real temperature. It simply alters the transition probability function and by doing so allows noise to be introduced into the system.

### 3.3. *Simulation parameters*

The current simulations were performed on a 250,000-site two-dimensional triangular lattice with first- and second-nearest-neighbor interactions. The temperature was set to $0.5\gamma_0/kT$, where $\gamma_0$ is the minimum grain boundary energy in the system, in the same units as k$T$. This temperature is low enough to prevent boundaries from disordering but high enough to minimize lattice pinning. In order to minimize finite size effects, periodic boundary conditions were imposed. To approximate a continuum crystallographic texture, $Q = 999$ different, discrete orientations were allowed. A specialized algorithm [30] was used to increase the time efficiency of the simulations. Numerical data points represent the average of 10 independent simulation runs.

## 4. ANISOTROPIC GRAIN GROWTH: RANDOM TEXTURE

For the first examination of texture and boundary character evolution, we choose the simplest system: a randomly textured, single-phase polycrystal. Each grain in the initial structure is assigned a crystallographic orientation from a list of 999 orientations, randomly distributed in Euler space. The grain boundary MDFs of these initial structures match the analytical solution for the MDF of a randomly textured polycrystal, known as the Mackenzie distribution (shown as the solid line in Fig. 4) [31]. Note that, in three-dimensional crystallography, a randomly textured polycrystal does not possess a uniform distribution of grain boundary misorientations. Because the misorientation angle results from the convolution of two random three-dimensional variables, it is easiest to achieve a misorientation near some mean angle, and low misorientations (requiring several particular relationships between orientation variables) are rare. This is quite different from one-dimensional (scalar) orientations (i.e., all [001] tilt boundaries), in which the MDF is uniform; likewise, the evolution of such systems is fundamentally different [11]. The characteristics of the Mackenzie distribution, such as a maximum misorientation of 62.8° and a peak in frequency at 45°, are a result of the cubic symmetry of the orientation space [31].

The misorientation of each of the 498,501 possible boundaries in the system is calculated, and the boundary energies and mobilities are assigned using equation (2) with $\theta_m = 15°$, 30° or 45°; these values are chosen to examine the dependence of the results on the cut-off between high- and low-angle boundaries. The randomly textured initial structures are evolved for $10^4$ MCSS (typically a grain area increase of four orders of magnitude).

### 4.1. *Microstructure and kinetics*

Figure 1 shows a snapshot of the microstructure of a randomly textured system undergoing grain growth. Geometrically, the structure varies from the isotropic case in its triple-junction angles, which are not uniformly 120°. This is expected in the presence of anisotropic boundary energies, since a force balance of unequal surface tensions requires unequal vertex angles [32]. However, the grain topology is typical of

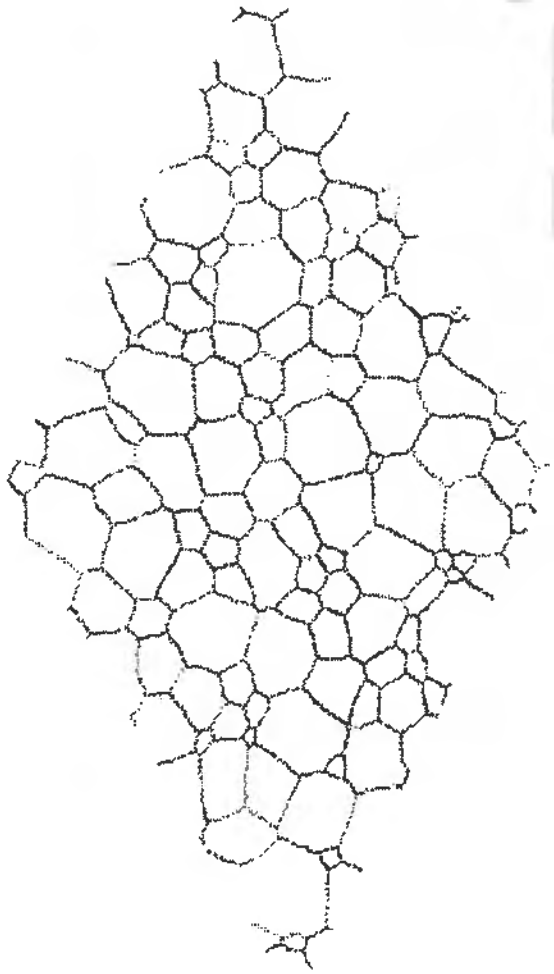

Fig. 1. Typical microstructure during grain growth from an initial random texture. Grain boundaries are shaded according to misorientation angle; high-angle boundaries are darker, low-angle boundaries are lighter. Grain boundary energy and mobility are given by equation (2) with $\theta_m = 30°$, and the system was evolved from a $500^2$-site random structure for 1000 MCSS. Note that the grain topology appears similar to that for isotropic, normal grain growth.

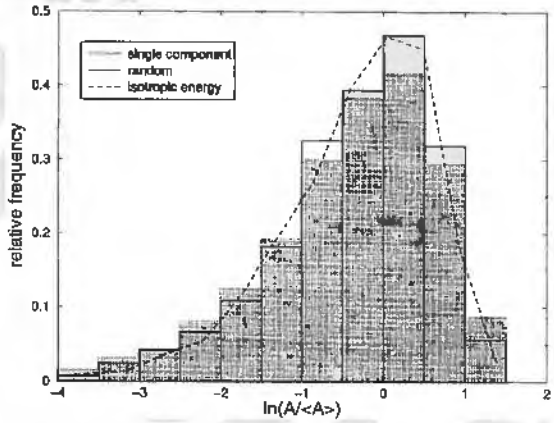


Fig. 2. Grain area distributions during grain growth. Systems with random crystallographic texture produce the same grain area distribution as normal grain growth (isotropic boundary properties and no texture). Systems with a single texture component produce a grain area distribution that is weighted towards small grains. All distributions were measured at $t = 1000$ MCSS. The isotropic and random texture distributions are steady-state; however, there is some evidence that the single-component texture system may not reach a steady-state area distribution.

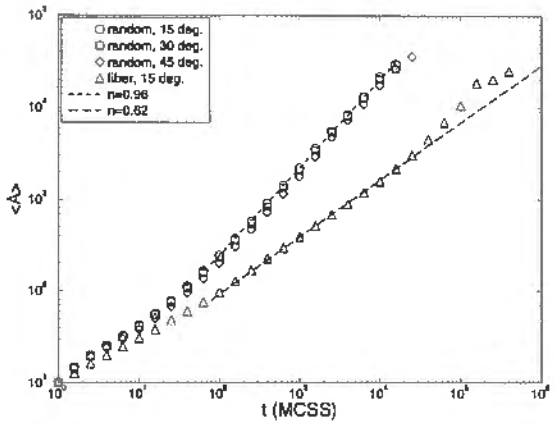


Fig. 3. Time evolution of mean grain area during grain growth in textured polycrystals. Polycrystals with random texture exhibit power-law growth with the normal grain growth exponent $n = 0.96$ (dotted line), independent of the value of $\theta_m$ in equation (2). Polycrystals with a single-component texture follow power-law growth with a decreased exponent $n = 0.62$ (dashed line).

normal grain growth, with triconnected grain vertices and an average of six sides per grain. Because topology governs fundamental grain growth processes, the system evolves very similarly to an isotropic system. The grain size distribution is identical to that produced by isotropic grain growth (Fig. 2). The area kinetics (Fig. 3) are also consistent with isotropic grain growth, as is the steady-state growth exponent for grain area, $n \sim 1$. Interestingly, the grain size distribution and growth kinetics are independent of the value of $\theta_m$ in equation (2).

### 4.2. *MDFs: influence of boundary energy*

During grain growth the MDF changes from the initial Mackenzie distribution to reflect the influence of the anisotropic properties of the boundaries. After an initial transient period (typically 1000 MCSS) the MDF reaches a steady state. Figure 4 compares the initial Mackenzie MDF and the steady-state MDF (averaged over 10 independent trials) for systems with $\theta_m = 15°$, 30° and 45°. The general shapes of the distributions are similar, although some enhancement in boundary frequency is noticeable at misorientations less than $\theta_m$, with a commensurate decrease at misorientations above $\theta_m$. The effect is more noticeable for higher values of $\theta_m$.

What is the cause of this increase in low-angle boundaries? Because low-angle boundaries have correspondingly low mobilities, they move more slowly and may simply persist in the system longer than

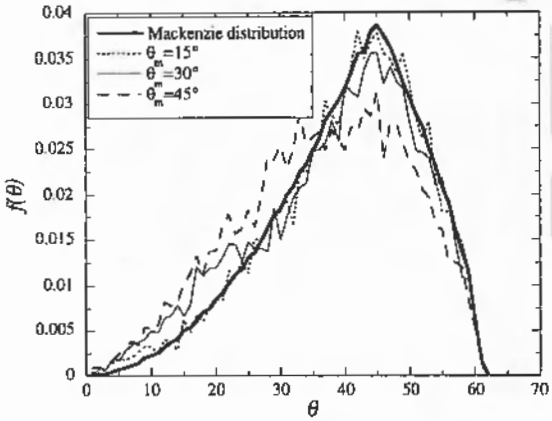


Fig. 4. Steady-state grain boundary misorientation distributions for polycrystals with random initial texture and grain boundary energy and mobility given by equation (2) with $\theta_m = 15°$, 30° and 45°. The initial distribution is the Mackenzie distribution (heavy solid line). Note that the steady-state distributions show some enhancement in frequency for misorientations below $\theta_m$ with a commensurate decrease above $\theta_m$.

high-angle boundaries. We tested this hypothesis by repeating the simulations with boundary energy given by equation (2) but isotropic reduced mobility, $M = 1$. The MDFs produced were identical to those generated with the anisotropic mobilities, indicating that energy is more important than mobility in determining the steady-state MDF. The MDF is not kinetically constrained by mobility.

It is possible that low-energy boundaries are preserved because they decrease the global system free energy. However, in the Potts model with uniform mobility, all processes that decrease system energy are accepted with the same probability [equation (5)], and all transitions are performed based on local interactions. Thus, there is no mechanism to preserve low-energy boundaries at the expense of high-energy boundaries. Since the uniform mobility simulations show low-angle boundary enhancement, local, and not global, energy minimization must provide the mechanism.

Therefore, we must conceive of local changes in microstructure that may enhance low-angle boundary lengths. Consider a grain boundary segment between two triple junctions. In the isotropic case [Fig. 5(a)], all boundary segments have the same surface tension ($\gamma = 1$), and all triple-junction angles are 120°. If the central boundary is replaced by a low-energy boundary, keeping the endpoints and energies of the other boundaries fixed [Fig. 5(b)], the terminal angles open and the central boundary lengthens. We can determine the change in length using the surface tension balance at the trijunctions. Comparing the isotropic trijunction [Fig. 5(c)] with the anisotropic junction [Fig. 5(d)], it is apparent that at each triple junction the increase in length of the low-energy boundary is

$$\Delta l = c\left[\frac{1}{2} - \frac{\gamma(\theta)}{2}\right], \tag{7}$$

where $c$ is a proportionality constant and $\gamma(\theta)$ is given by equation (2). For a unit boundary with two terminal triple junctions, the new length is $l = 1 + 2\Delta l$. Now we multiply this relative increase in boundary length by the initial amount of each boundary type $L_0(\theta)$ to find the total amount of each boundary:

$$L(\theta) = L_0(\theta)\{1 + c[1-\gamma(\theta)]\}. \tag{8}$$

We then divide through by the initial total amount of boundary [the integral of $L_0(\theta)$] to find

$$g(\theta) = f_0(\theta)\{1 + c[1-\gamma(\theta)]\}, \tag{9}$$

where $f_0(\theta)$ is the Mackenzie distribution. Normalizing $g(\theta)$ by its integral gives the final frequency distribution

$$f(\theta) = \frac{f_0(\theta)\{1 + c[1-\gamma(\theta)]\}}{\int f_0(\theta)\{1 + c[1-\gamma(\theta)]\}\, d\theta}. \tag{10}$$

Equation (10) provides an excellent fit to the steady-state MDFs for all $\theta_m$, as shown in Fig. 6. Note that there is only one adjustable parameter, $c$. For $\theta_m = 15°$, 30° and 45°, the best fit is found for $c \sim 6$, indicating some universality to the scaling behavior.

The quality of the fit is quite surprising considering the simplifications made in the analysis. This analysis assumes only one type of triple junction, two high-angle boundaries meeting a single low-angle boundary. However, in a polycrystal other triple junctions are certainly present, and they possess a variety of boundary energies. Triple junctions with more than one low-angle boundary become more prevalent as the frequency of low-angle boundaries increases, which is the case for misorientations near $\theta_m$ particularly as $\theta_m$ increases. This likely accounts for equation (10)'s underestimation of boundary frequency near $\theta_m$ for $\theta_m = 30°$ and 45°. However, equation (10)'s excellent first-order fit illustrates how local geometry can enhance the lengths of low-energy boundaries.

One implication of this analysis is that the enhancement in low-misorientation boundary frequency is due to an increase in the length, and not the number, of such boundaries. The MDF data in Figs 4 and 6 are length-weighted; they plot the length of each boundary type relative to the total boundary length in the system. For the same structures, the number-weighted MDFs (plotting the number of each boundary type relative to the number of boundaries) show a minimal increase in low-angle boundaries. Thus, most of the gain in low-misorientation boundaries is caused by the lengthening of these boundaries and not by their proliferation.

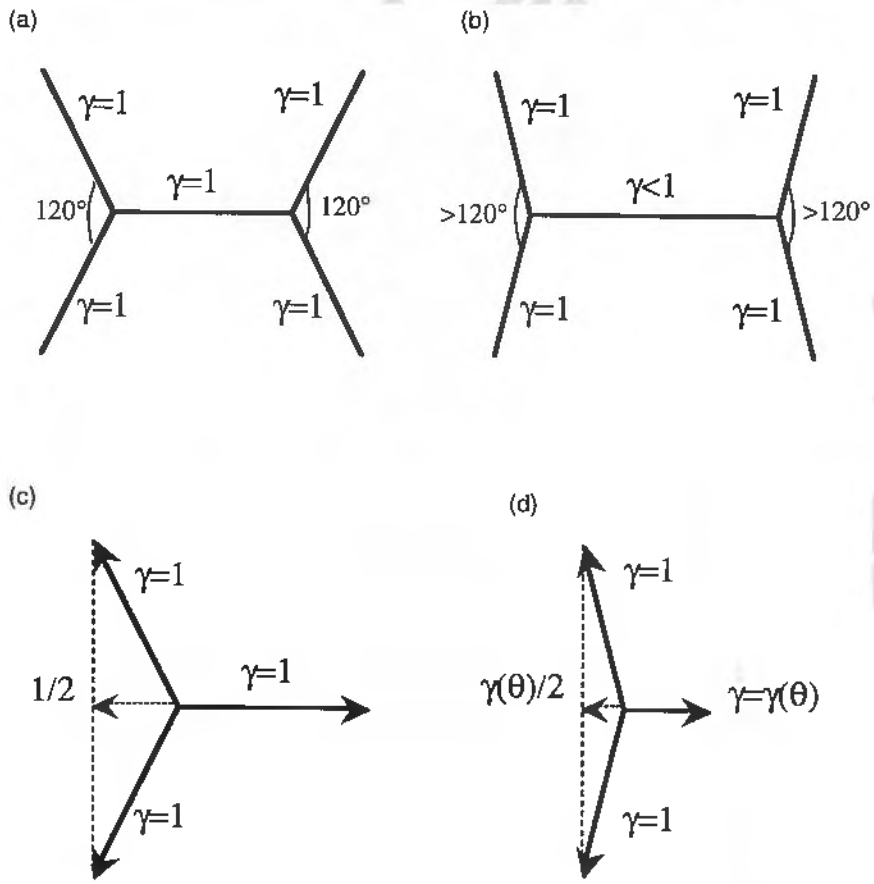


Fig. 5. Geometric lengthening of low-energy grain boundaries. (a) In the isotropic case all boundary segments have the same surface tension ($\gamma = 1$), and all triple-junction angles are 120°. (b) If the central boundary is replaced by a low-energy boundary ($\gamma<1$) holding other boundary endpoints fixed, the terminal angles open and the central boundary lengthens. The surface tension balances for (c), an isotropic triple junction, and (d), an anisotropic junction, show that the low-energy boundary increases by an amount proportional to $1/2-\gamma(\theta)/2$ at each triple junction.

There is little experimental data on the microstructural evolution of random textures, although Wantanbe *et al.* [33] show that grain growth of rapidly solidified Fe–Si alloys with initially random textures leads to a bias in the MDF at low misorientation angles.

The development of a steady-state MDF is not inevitable; it depends on the type of texture present. In the next section we consider a case that allows a continuous reduction in the average misorientation during grain growth.

## 5. GRAIN GROWTH OF A SINGLE-COMPONENT TEXTURE

To contrast with the randomly textured case, we selected a system with a high degree of bulk texture. Each grain in the initial structure is assigned an orientation from a Gaussian distribution of orientations around {111}⟨100⟩. Because all orientations are close to a common reference axis, it is easy to form a boundary at or below the mean misorientation, but it is harder to find grains that can form a high-angle boundary with each other. Thus, although the orientation distribution is Gaussian about {111}⟨100⟩, the grain boundary misorientation distribution is asymmetric; it is skewed towards low misorientation angles, and its median is less than its mean misorientation of 2°.

The single-component MDF is qualitatively similar to MDFs observed experimentally in subgrain structures by Hughes *et al.* [34]. This is reasonable, since subgrain structures represent orientation perturbations from an initial common orientation (the original grain orientation). The orientation distributions of the two systems differ, however, which causes a quantitative difference in their MDFs. The single-component MDF is more sharply peaked than the subgrain MDF.

The misorientation of each boundary in the system is calculated, and the boundary energy and mobility are assigned using equation (2) with $\theta_m = 15°$. The single-component texture structures are evolved for

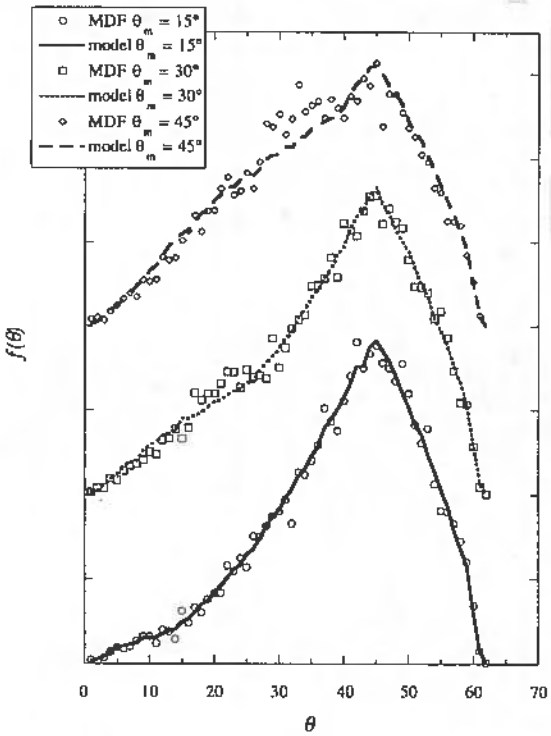


Fig. 6. Comparison between model and observed steady-state grain boundary misorientation distributions for polycrystals with random initial texture and grain boundary energy and mobility given by equation (2) with $\theta_m = 15°$, 30° and 45°. The model misorientation distribution is given by equation (10), with $c \sim 6$ producing the best fit in all cases. The model accurately reproduces the observed distributions, with only slight underestimation of misorientation frequency near $\theta_m$ for $\theta_m = 30°$ and 45°. Curves are displaced along the $y$-axis for clarity.

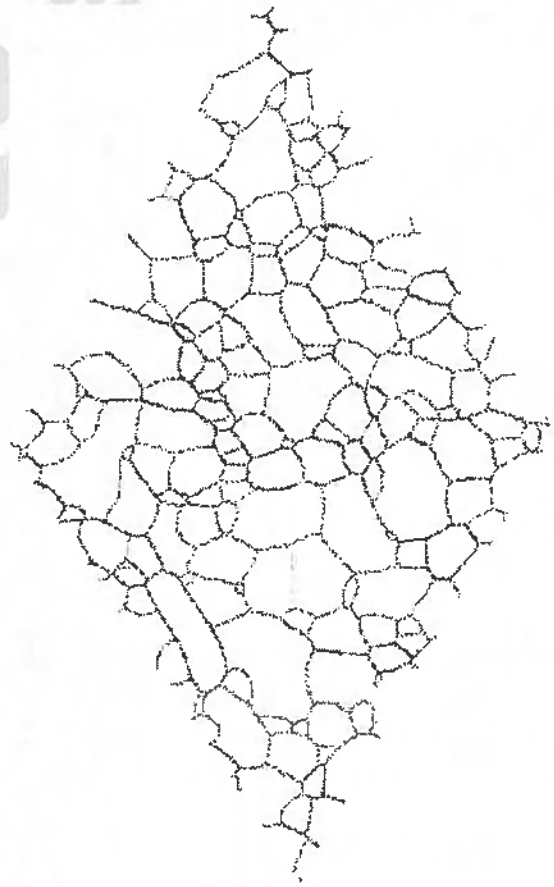

Fig. 7. Typical microstructure during grain growth from a single-component initial texture. Grain boundaries are shaded according to misorientation angle; high-angle boundaries are darker, low-angle boundaries are lighter. Grain boundary energy and mobility are given by equation (2) with $\theta_m = 15°$, and the system was evolved from a $500^2$-site random structure for 10,000 MCSS. Note the presence of few-sided, highly curved grains and of stable four-grain junctions (quadrijunctions).

$10^5$ MCSS (typically a grain area increase of four orders of magnitude).

### 5.1. *Microstructure and kinetics*

Figure 7 shows a snapshot of the microstructure during evolution of the single-component texture. The color of the boundaries has been adjusted so that white represents zero misorientation and black is the maximum misorientation in the microstructure. The microstructural morphology is significantly different from that of the random texture (compare Fig. 1 and Fig. 7). Because all boundaries in the system are far below the high-angle cutoff $\theta_m$ in equation (2), the boundary energy and mobility vary greatly with small changes in misorientation. Low-mobility boundaries accumulate curvature and can temporarily stabilize few-sided grains. Triple-junction angles are far from 120°, and thermodynamically stable four-grain junctions (quadrijunctions) also appear [35]. Because the topology of the microstructure is different from that of the isotropic case, the details of microstructural evolution are also altered. As shown in Fig. 2, stabilization of small grains by low-mobility boundaries skews the grain area distribution towards small areas. Grain growth kinetics (see Fig. 3) are slower than for random texture, with a steady-state area growth exponent $n = 0.62$.

It is interesting to observe that there are several grains surrounded by high-angle boundaries in Fig. 7. These grains are not among the largest in the system, even though their boundaries are much more mobile than average. Because their boundaries are high in energy, these grains are not favored to grow. In fact, we do not observe any abnormal or discontinuous grain growth events in these systems, in agreement with previous studies which indicate that grains require an energetic advantage to grow abnormally [12].

### 5.2. *Continuously evolving MDFs*

The persistence of grains with low-angle, low-mobility boundaries biases the structure towards those boundaries, causing the MDF to narrow and shift left,

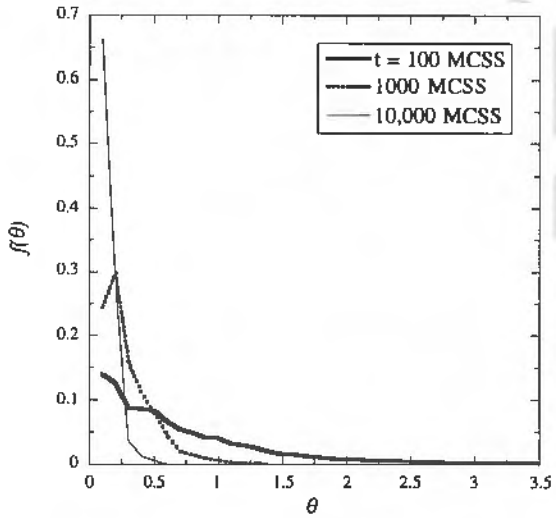


Fig. 8. Grain boundary misorientation distributions for polycrystals with single-component initial texture and grain boundary energy and mobility given by equation (2) with $\theta_m = 15°$. Due to the accumulation of low-angle, low-mobility boundaries, the distributions narrow and shift left with time, and no steady-state distribution is observed.

as shown in Fig. 8. The mean and the standard deviation of the MDF decrease continuously, as shown in Fig. 9, and there is no steady-state MDF. A similar decrease in the mean misorientation and a sharpening of crystallographic texture have been observed experimentally during the annealing of strongly textured materials for both grains [36] and subgrains [24].

In the randomly textured polycrystal, the steady-state MDF occurs because, when two grains meet during growth, the resulting boundary is likely to be near the mean misorientation (i.e., high angle). Any low-angle, low-mobility boundary that does form is likely to be surrounded by high-angle boundaries, which can freely sweep past less mobile boundaries. In contrast,

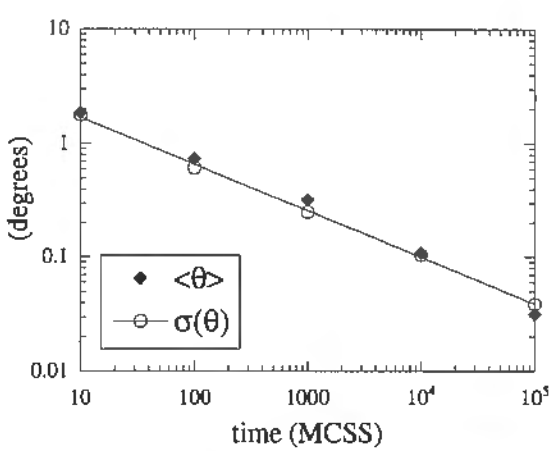


Fig. 9. Evolution of the mean misorientation angle $\langle\theta\rangle$ and the standard deviation of the misorientation distribution $\sigma(\theta)$ during evolution of polycrystals with a single-component texture. Both $\langle\theta\rangle$ and $\sigma(\theta)$ decrease in time by a power law with exponent $p = -0.41$ (solid line).

in the single-component texture all grains have orientations near the reference {111}⟨100⟩ axis. Thus, as a grain grows, the new neighbors it meets are likely to be similarly oriented to itself (i.e., form a low-angle boundary). Likewise, low-mobility boundaries are likely to be surrounded by other low-mobility boundaries, allowing them to persist. The mechanism for shifting and narrowing the MDF is probably the formation and augmentation of such low-mobility boundary clusters. Our simulations support this hypothesis; single-component texture microstructures are characterized by a percolating network of similarly oriented grains with very low misorientation boundaries between them.

In the single-component texture, grain growth is considerably slower than for normal grain growth, with a time exponent $n = 0.61$, as shown in Fig. 3. The decreased exponent does not reflect either a different grain growth mode or simulation lattice pinning, but rather is a consequence of the increase in low-mobility boundaries as coarsening progresses [24]. At every time step, the amount of grain growth is scaled by the average boundary mobility. The average mobility is determined by the average boundary misorientation, which decreases with time by a power law with exponent $p = -0.41$, as shown in Fig. 9. Consider the mean field analysis of grain growth by Burke and Turnbull [37]. The rate of change of the average grain size, $\langle R\rangle$, is given by

$$\frac{d\langle R\rangle}{dt} = \frac{c_1\langle M\rangle}{\langle R\rangle}, \tag{11}$$

where $\langle M\rangle$ is the average reduced mobility of the grain boundaries and $c_1$ is a geometrical constant. In our simulations $\langle M\rangle$ is a function of the mean misorientation $\langle\theta\rangle$ as given by equation (2), but for the moment assume a simple linear dependence (a reasonable approximation in this small-angle limit), so that

$$\langle M\rangle \approx c_2\langle\theta\rangle, \tag{12}$$

where $c_2$ is a constant. From the simulations we observe that

$$\langle\theta\rangle = c_3 t^p, \tag{13}$$

where $c_3$ is a constant. Substituting equations (12) and (13) into (11) gives

$$\frac{d\langle R\rangle}{dt} = \frac{c_1 c_2 c_3 t^p}{\langle R\rangle} \tag{14}$$

and integration then yields

$$\langle A\rangle - \langle A_0\rangle = Ct^{1+p}, \tag{15}$$

where the average grain area $\langle A\rangle \sim \langle R\rangle^2$, $\langle A_0\rangle$ is the initial grain area, and $C$ is a constant combining proportionality and integration constants. Thus analysis predicts that the grain growth exponent, $n$, is related to the power-law exponent of average misorientation, $p$, by the expression:

$$n = 1 + p. \tag{16}$$

The simulation agrees with this prediction, with $p = -0.41$ and $n = 0.62$. It should be noted if one goes back and replaces equation (12) with equation (2) the derivation is more complicated, but we recover essentially the same formula.

This result shows that kinetic exponents measured in the simulation are self-consistent and do not arise from lattice pinning. While in the random texture case the number of low-mobility boundaries is insufficient to influence microstructure or kinetics, in the single-component texture the prevalence of such boundaries controls both the microstructural development and the time scale for evolution.

Proving the time exponents to be self-consistent does not explain why they take the particular values observed. An area for future study is to derive a model for evolution of the single-component MDF that can predict the time exponent for mean misorientation. Grain growth exponents of $n<1$ are commonly observed experimentally, and $n\sim 2/3$ is often cited. It is possible that such depressed exponents are a result of decreasing average boundary mobility arising from the tightening of crystallographic texture or from other effects such as solute accumulation.

## 6. CONCLUSIONS

In order to study the development of texture and boundary character during annealing, full three-dimensional grain crystallography and realistic, crystallographically mediated grain boundary properties were incoporated into a finite temperature Monte Carlo Potts model for grain growth.

Systems with similar initial microstructures but different textures exhibit markedly different behavior during grain growth. Microstructures with random textures maintain normal grain topology and evolve in a normal fashion. The grain size distribution is statistically equivalent to that of isotropic grain growth, and grain area evolution kinetics follow the usual power law with exponent $n = 0.96$. While texture remains random in these systems, the boundary character distribution evolves to a steady state that favors low-misorientation-angle boundaries. To first order, the increase in low-angle boundaries is geometrical; changes in triple-junction angles cause low-energy boundaries to lengthen, but their frequency does not increase.

In contrast, microstructures with a strong single-component texture develop four-grain junctions and highly curved grain boundaries. This change in topology causes a change in evolution behavior. The grain size distribution is skewed towards small grains, and grain growth kinetics are depressed, with a power-law exponent of $n = 0.62$. Both the texture and the misorientation distribution sharpen, and no steady state is observed. Formation and growth of clusters of low-mobility boundaries cause the boundary misorientation distribution to narrow and shift to low angles, with the mean and standard deviation of the distribution decreasing as a power law with time exponent $p = -0.41$. Since the grain growth exponent $n = 1 + p$, the accompanying decrease in mean boundary mobility causes growth to slow. The dependence of the growth exponent on average boundary mobility may explain experimental observations of grain growth exponents less than unity.

Experimental data for the evolution of the boundary character during grain growth are scarce. However, these results are in good agreement with typical observations that low-angle boundaries increase during annealing. While often seen in experiments, abnormal grain growth did not occur in these simulations.

*Acknowledgements*—Thanks to Dr A. W. Godfrey for discussions and providing orientation handling subroutines. MAM is grateful for support through a Newman Scholarship at University College Dublin, Ireland. GNH appreciates support from Kettering University and Sandia National Laboratories for sabbatical leave. This work was performed at Sandia National Laboratories, supported by the US Department of Energy under contract number DE-AC04-94AL85000 and by the Office of Basic Energy Sciences New Initiative program.

## REFERENCES

1. Schwartz, A. J. and King, W. E., *JOM*, 1998, **50**(2), 50.
2. Palumbo, G. et al., *Mater. Res. Soc. Symp. Proc.*, 1997, **458**, 273.
3. Palumbo, G., Lehockey, E. M. and Lin, P., *JOM*, 1998, **50**(2), 40.
4. Adams, B. L., Wright, S. I. and Kunze, K., *Met. Trans.*, 1993, **A24**(4), 819.
5. Miodownik, M., Godfrey, A. W., Holm, E. A. and Hughes, D. A., *Acta metall. mater.*, 1999, **47**(9), 2661.
6. Anderson, M. P., Srolovitz, D. J., Grest, G. S. and Sahni, P. S., *Acta metall.*, 1984, **32**(5), 783.
7. Frost, H., Thompson, C. V. and Walton, D. T., in *Grain Growth in Polycrystalline Materials*, ed. G. Abbruzzese and P. Brosso. Trans Tech Publications, Brookfield, VT, 1992, p. 543.
8. Weaire, D. and Kermode, J. P., *Phil. Mag. B*, 1983, **48**, 245.
9. Chen, L. -Q. and Wang, Y. -Z., *JOM*, 1996, **11**, 48.
10. Raabe, D., in *Grain Growth in Polycrystalline Materials III*, ed. H. Weiland, B. L. Adams and A. D. Rollett. TMS, Warrendale, PA, 1998, p. 179.
11. Grest, G. S., Srolovitz, D. J. and Anderson, M. P., *Acta metall.*, 1985, **33**(3), 509.
12. Rollett, A. D., Srolovitz, D. J. and Anderson, M. P., *Acta metall.*, 1989, **37**(4), 1227.

13. Saito, Y. and Enomoto, M., *ISIJ Int.*, 1992, **32**(3), 267.
14. Hinz, D. C. and Szpunar, J. A., *Phys. Rev. B*, 1995, **52**, 9900.
15. Mehnert, K. and Klimanek, P., *Comp. Mater. Sci.*, 1996, 7, 103.
16. Ono, N., Kimura, K. and Watanabe, T., *Acta mater.*, 1999, **47**, 1007.
17. Lee, H. N., Ryoo, H. S. and Hwang, S. K., *Mater. Sci. Eng.*, 2000, **A281**, 176.
18. Kronberg, M. L. and Wilson, F. H., *Trans. AIME*, 1949, **185**, 501.
19. Sutton, A. P. and Balluffi, R. W., *Interfaces in Crystalline Materials*. Oxford Science Publications, Oxford, 1995.
20. Brandon, D. G., *Acta metall.*, 1966, **14**, 1479.
21. Read, W. T. and Shockley, W., *Phys. Rev. B*, 1950, **78**, 275.
22. Gottstein, G., Molodov, D. A. and Shvindlerman, L. S., in *Grain Growth in Polycrystalline Materials III*, ed. H. Weiland, B. L. Adams and A. D. Rollett. TMS, Warrendale, PA, 1998, p. 373.
23. Molodov, D. A., Gottstein, G., Heringhaus, F. and Shvindlerman, L. S., *Acta mater.*, 1998, **46**(16), 5627.
24. Huang, Y. and Humphreys, F. J., *Acta mater.*, 2000, **48**, 2017.
25. Raabe, D., *Acta mater.*, 2000, **48**, 1617.
26. Holm, E. A., Miodownik, M. A. and Cahn, J. W., in press.
27. Holm, E. A., Glazier, J. A., Srolovitz, D. J. and Grest, G. S., *Phys. Rev. A*, 1991, **43**(6), 2662.
28. Miodownik, M. A., Martin, J. W. and Cerezo, A., *Phil. Mag. A*, 1999, **79**, 203.
29. Holm, E. A., Srolovitz, D. J. and Cahn, J. W., *Acta metall. mater.*, 1993, 41(4), 1119.
30. Hassold, G. N. and Holm, E. A., *Comput. Phys.*, 1993, 7(1), 97.
31. Mackenzie, J. K., *Biometrika*, 1958, **45**, 229.
32. Cottrel, A. H., *The Mechanical Properties of Matter*. Wiley, New York, 1964.
33. Watanabe, T., Fujii, H., Oikawa, H. and Arai, K. I., *Acta mater.*, 1989, **37**, 941.
34. Hughes, D. A., Chrzan, D. C., Liu, Q. and Hansen, N., *Phys. Rev. Lett.*, 1998, **81**, 4664.
35. Cahn, J. W., *Acta metall. mater.*, 1991, **39**(10), 2189.
36. Vogel, S., Klimanek, P., Juul Jensen, D. and Richter, H., *Scripta mater.*, 1996, **34**, 1225.
37. Burke, J. E. and Turnbull, D., *Prog. Met. Phys.*, 1952, **3**, 220.